THE EFFECT OF MANGANESE ON Fe-RICH INTERMETALLIC PHASES IN PROGRESSIVE SECONDARY AlSi7Mg0.6 ALLOY

UDC:669.715
Original scientific paper https://doi.org/10.18485/aeletters.2022.7.3.2

Lucia Pastierovičová[1*], Lenka Kuchariková[1], Eva Tillová[1], Mária Chalupová[1], Miroslaw Bonek[2]

[1] University of Žilina, Faculty of Mechanical Engineering, Department of Materials Engineering, Univerzitná 8215/1, 010 26 Žilina, Slovak Republic
[2] Faculty of Mechanical Engineering, Department of Materials Engineering and Biomaterials, Silesian University of Technology, Konarskiego 18A Street, 44-100 Gliwice, Poland

Abstract:
The contribution describes the major problem with the secondary (recycled) alloys as the presence of unwanted elements due to the remelting of Al-scrap negatively affecting the quality of AlSi7Mg0.6 cast alloy. Iron is the most harmful impurity in the secondary Al-Si alloys, leading to the formation of β-Fe-rich (Al_5FeSi) intermetallic phases that promotes forming of casting defects such as porosity and shrinkage by its needle-like shape. Suitable neutralizer alloying elements, such as Mn, influence the formation of Fe-needle-like phases and lead to the formation of less harmful Mn-containing α-Fe-rich phases. To optimize the morphology and properties of alloys, it is necessary to study the effects of individual alloying elements. Therefore, this study is focused on the effect of Mn addition on Fe-rich intermetallic phases and casting defects, thus the evaluation of its shape and distribution in AlSi7Mg0.6 secondary alloy.

ARTICLE HISTORY
Received: 13.07.2022.
Accepted: 22.09.2022.
Available: 30.09.2022.

KEYWORDS
Secondary aluminium alloy, iron content, quantitative analysis, porosity, Fe-rich phases, microstructural changes, sludge

1. INTRODUCTION

Aluminium is vital for Europe providing a solution to many social and economic challenges that Europe faces in its efforts to build a more sustainable and resource-efficient economy. Aluminium is infinitely recyclable because its essential properties remain unchanged after multiple recycling loops. In addition, the low energy levels required for recycling compared with its initial manufacture make it an “energy bank” [1].

Aluminium has many different applications but it is particularly important in transport, as it reduces the carbon footprint of cars and trucks (on average 140 kg in every new car). When these products reach the end of their life cycle, the material can be easily recycled and give life to a new product. Due to those qualities, 75 % of all the aluminium ever produced is still in use today [1].

More than half of all aluminium currently produced in the European Union comes from recycled (secondary) aluminium produced by refineries and smelters, which shows that Europe is already the world's largest recycler per capita and this trend is increasing Fig. 1) [1, 2].

Recycled (secondary) aluminium is produced from recycled aluminium originating from various forms of aluminium scrap and consists of:

- End-of-life aluminium scrap;
- End-of-life aluminium not collected (e.g. ending up in landfill);
- End-of-life aluminium (collected and recycled) [3].

Thousands of scrap dealers worldwide collect recycled aluminium, segregate it by type and grade and repackage it for shipment. After that aluminium scrap is sent to a recycling facility, where it is shredded, melted, and recast.

*CONTACT: L. Pastierovičová, e-mail: lucia.pastierovicova@fstroj.uniza.sk

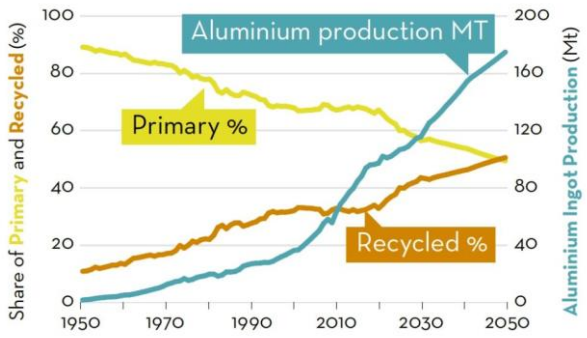

Fig. 1. Share of primary and recycled aluminium through 2050 [4]

The aluminium industry is an energy-intensive process using elevated temperatures with a significant environmental impact. Therefore, companies are focused on minimizing the production of primary-ore aluminium alloy components and replacing them with the secondary-recycled alloys as they can berecycled indefinitely without losing their intrinsic properties.

Aluminium recycling has many benefits including energy savings of up to 95 % and 85 % less CO_2 emission compared to primary production. In this regard, a study of recycling in the aluminium industry is of a high importance, especially in view of the increasing concerns about greenhouse gas emissions, global warming, and the rising tendency of fuel prices [1-2, 3-7].

Nowadays, it is estimated that 60 % of the metal used in automobiles is comprised of recycled aluminium. This percentage is expected to increase steadily over the next 20 years, and recycled aluminum should make up to 90% of the aluminum content in a car. Aluminum's light weight can improve the performance of any vehicle using the same powertrain and equipment now used in heavier vehicles that require a lot of steel [2-3].

Al-Si-based alloys are the most representative recycled alloys for cast applications due to their high specific strength, good castability, corrosion resistance and so on, used as a replacement for steel components in automotive and aerospace industries [8-11].

However, the properties of Al-Si alloys are highly influenced by their chemical composition since containing elements (Si, Mg, Mn) that are present either intentionally to improve the properties of the alloy or non-intentionally. The major problem with recycled alloys is the presence of undesirable elements due to the remelting of Al-scrap. It is very difficult to eliminate their negative effects on Al-alloys. Iron is considered as the most harmful impurity in the recycled Al-Si alloys, leading to the formation of Fe-rich intermetallic phasessuchas β-Fe-rich phase (β-Al_5FeSi) or α-Fe-rich phase (α-$Al_{15}(FeMn)_3Si_2$), whose morphology influences the properties of Al-Si castings [5, 8-14].

The Al_5FeSi phase is a hard and brittle phase, precipitate of a 3D platelet form (appearing as needles in 2D sections) that by its shape acts as a stress enhancer and blocks the flow of liquid in interdendritic areas during the solidification, as another research work by Brueckner-Foit [15] confirmed. The Al_5FeSi phases promote forming of casting defects, such as porosity and shrinkage due to the precipitation of long and thick needles/platelets. It has been suggested that porosity increases with iron content since the Al_5FeSi platelets block the interdendritic flow channels. Alternatively, Al_5FeSi platelets have been proposed to nucleate the eutectic silicon, causing changes to microstructural permeability [9].

The α-$Al_{15}(FeMn)_3Si_2$ phases appear during the eutectic solidification with α-Al and commonly have a skeleton-like or Chinese script-like morphology. It has been proven that these morphologies of the α-$Al_{15}(FeMn)_3Si_2$ phase can reduce the harmful effects of Fe-rich needles (Al_5FeSi) to a minimum due to the shape and size of α-$Al_{15}(FeMn)_3Si_2$ [12, 15, 16].

Suitable neutralizer elements, such as Mn, influence the formation of the β-Fe-rich phase [15]. The Mn addition leads to formation of Mn-containing intermetallic phases, such as $Al_{15}(FeMn)_3Si_2$. The addition of Mn converts the needle-like β-Fe phases into α-Fe phases in Chinese script or skeleton-like form that does not initiate cracks like the β-Al_5FeSi and thus allows producing an alloy with properties adjusted to applications [16-18]. The addition of Mn to Fe-containing Al-Si cast alloys has also been credited with decreasing porosity [19]. The amount of Mn needed to neutralize iron is not well established. A common ‘‘rule of thumb’’ appears to be a ratio between the Fe and Mn concentrations of 2:1 [9, 17, 19, 20].

On the other hand, with a slower cooling rate, polyhedral/star-like shaped α-particles known as the sludge phases may nucleate as primary particles [16, 17, 20-23]. According to the research work of [21], sludgecontrols the formation of porosity to some extent when the porosity at the fracture surfaces increases in Fe-rich alloys, modified to the sludge. The nucleation propensity of Fe-rich primary particles in an Al-Si alloy can be

estimated using a sludge factor combining the influence of Fe, Mn and Cr. The generally accepted empirical SF equation, expressed by Dunn [14]as:

$$SF = wt.\ \%\ Fe + 2 \times wt.\ \%\ Mn + 3 \times wt.\ \%\ Cr \quad (1)$$

The SF may thus vary strongly depending on the chemical composition of the alloy; the higher the SF, the higher the amount of sludge present in the microstructure [24, 25].

To optimize properties in the secondary Al-Si cast alloys, it is necessary to study the effects of individual alloying elements, especially the influence of higher amounts of iron.

Therefore, this study is focused on the effect of Mn addition on the morphology of Fe-rich intermetallic phases and evaluation of its shape and distribution in the AlSi7Mg0.6 secondary alloy with an iron content higher than 1 %.

2. EXPERIMENTAL MATERIAL

The secondary AlSi7Mg0.6 (A357) cast alloy was used as the experimental material, supplied from the company UNEKO s.r.o., CZ. Two melts (alloy A and alloy B) were cast with 1.2 % wt. Fe. The 0.66 % wt. Mn (Fe/Mn = 2/1) was intentionally added into melt B. To increase the % Fe and % Mn content, AlFe75 and AlMn75 pre-alloys were used. The chemical composition, according to the delivery list, is shown in Table 1.

Table 1. Chemical composition of AlSi7Mg0.6 cast alloy [% wt.]

Alloy	Si	Fe	Cu	Mn	Mg	Ti	SF
A	7.27	1.26	0.02	0.01	0.55	0.12	1.34
B	7.04	1.24	0.01	0.66	0.54	0.11	2.62
In alloys A, B: Zn (<0,02); Ni (<0.02); Cr (<0.02); Pb (<0.05); Sn (<0.03); Na (<0.06); Sr (<0.02); Al (rest)							

From the individual experimental melts, experimental bars ø 20 x 300 mm were cast into sand moulds by the gravity casting method. The casting temperature was 750 °C and the refining temperature was 740 - 745 °C. The experimental alloys were not modified, grain refined, or heat treated. This type of material belongs to the group of aluminium alloys used especially for casting in mechanical, electrical engineering, automotive and aerospace industries etc. [16].

2.1 Experimental methodology

For microstructural analysis standard metallographic procedure was performed. Metallographic samples were cut from experimental bars using the MTH MIKRON 3000 automatic saw. Samples were liquid-cooled during the cutting to avoid thermal and mechanical effects on the structure. Next, the wet grinding on rough and soft grit sandpaper on a Tegra System from Struers was used. Polishing was performed to achieve a perfectly flattened surface on the Struers Op-S system. After each operation, the samples were rinsed with warm water and ethanol and dried in hot air. Prepared samples were etched by standard reagent 0.5 % HF, used for evaluation of microstructure by light microscope NEOPHOT 32 and scanning electron microscope VEGA LMU II. Samples were etched by reagent 95 % H_2SO_4, to highlight the Fe-rich phases required for quantitative analysis. Quantitative analysis of Fe-rich phases and porosity was performed by the NIS Elements software connected to the light microscope NEOPHOT 32. Each measured data is the average value of minimum 300 measured lengths of Fe-rich phases and pores.

3. RESULTS AND DISCUSSION

The representative microstructures of alloys A and B correspond to the hypoeutectic alloys are shown in Fig. 2.

The microstructure of both experimental alloys consists of dendrites α-phase (light grey), eutectic (mixture of α-matrix and spherical grey Si-phases) and various types of intermetallic phases. From the SEM observation (Fig. 3), the intermetallic phases were identified as:

- Al_5FeSi - dark grey needles (platelets);
- $Al_{15}(FeMn)_3Si_2$ - pale grey in the form of the Chinese script, resp. in a skeleton-like form;
- AlFeMnMgSi - sharp-edged particles;
- Mg_2Si - dark round particles.

In the microstructure of alloy B are found α-sludge phases, as well, due to the addition of Mn and Cr in a typical star-like shape with SF 2.62 according to Equation (1).

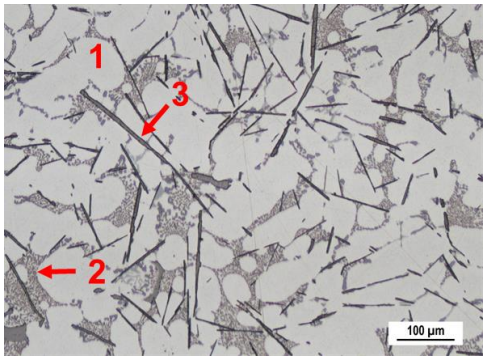

a) alloy A

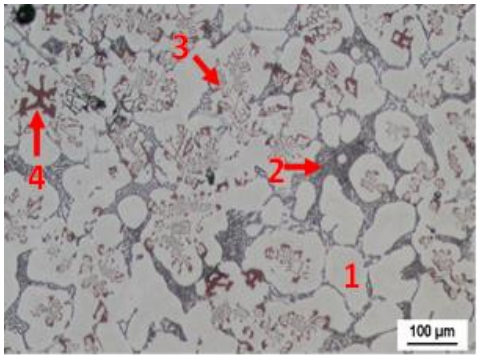

b) alloy B

Fig. 2. Microstructure of AlSi7Mg0.6 cast alloy; 1- α-phase, 2-eutectic, 3-Fe-intermetallic phases, 4-sludge phases; etch. 0.5 % HF

As shown in alloy A (Fig. 2a and 3a), the long, thick and needle-like Al_5FeSi phases are crystallized in alloy A without Mn. According to Seifeddine [20], at iron levels above 1 %, the Fe-needles precipitate as primary and result in extremely large structures independent of the cooling rate. In the microstructure of alloy B (Fig. 3b), this phase has a more rounded shape with a shorter length and is observed only locally.

With addition of Mn (0.66 wt. % - alloy B), the needle-like Al_5FeSi phase was replaced by a skeleton-like or Chinese script-like $Al_{15}(FeMn)_3Si_2$ phase (Fig. 2b and 3b), as confirmed by research works [12, 16 or 20].

The more compact α- $Al_{15}(FeMn)_3Si_2$ phase forms early in the solidification process and a large amount of iron is therefore consumed, reducing the iron content of the residual liquid and preventing the nucleation of β-Al_5FeSi platelets prior to the Al-Si eutectic. The $Al_{15}(FeMn)_3Si_2$ phase is more or less equiaxed and tends to form as dendrites (Fig. 2b and 3b). Additionally, sludge phases are also found in alloy B due to its chemical composition (Fig. 2b).

The AlFeMnMgSi intermetallic phases are present in both alloys in the form of sharp-edged particles and Mg_2Si phase in form of rounded black particles along the sides of the eutectic Si particles (Fig. 3a).

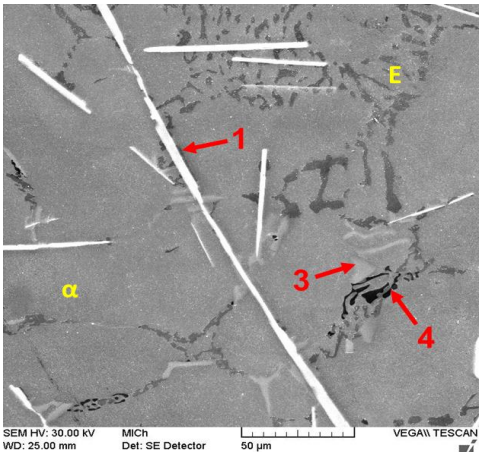

a) alloy A

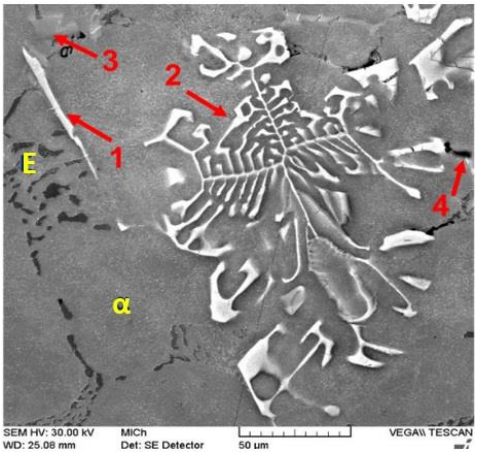

b) alloy B

Fig. 3. Intermetallic phases of AlSi7Mg0.6 alloy; 1- Al_5FeSi, 2- $Al_{15}(FeMn)_3Si_2$, 3- AlFeMnMgSi, 4- Mg_2Si, etch. 0.5 % HF, SEM

The quantitative analysis was mainly focused on the morphological and structural changes of Fe-phases caused by the addition of Mn. The amount of Fe-phases and the length and area fraction of the needle-like Al_5FeSi phase were measured (Fig. 4), since the iron leads to an increase in amount and size, especially of the Fe-rich phases in the form of needles [3,8].

Iron facilitates the formation of porosity, which seems to be related to formation and occurrence of the Fe-rich phases. The Fe-phases cause serious feeding difficulties during the solidification. The morphology of the Al_5FeSi phase blocks interdendritic flow channels, therefore, it is proposed that the higher iron content in the alloy is associated with higher levels of porosity, as well. Moreover, as mentioned before, the Al_5FeSi phase

promotes casting defects - porosity, therefore the pore size and porosity were measured as well.

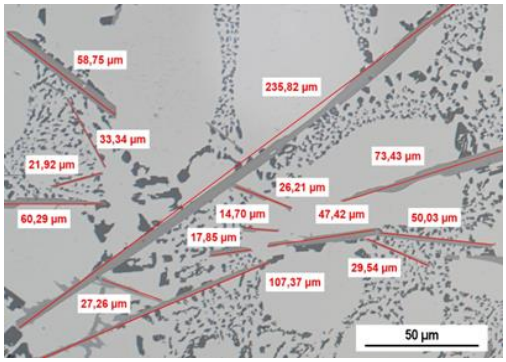

alloy A

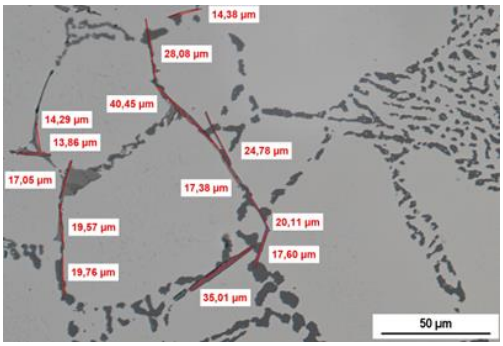

alloy B

Fig. 4. Quantitative analysis of Al_5FeSi phases in AlSi7Mg0.6 alloy, etch. 95 % H_2SO_4

The results of the quantitative analysis are presented in graphs in Fig. 5.

It is well known that the Mn and Fe content can influence the type, size, and ratio of different Fe intermetallic compounds. The area fraction of Al_5FeSi needles decreased from 3.5 % in alloy A to 0.9 % in alloy B (Fig. 5a) and in alloy B a phase $Al_{15}(FeMn)_3Si_2$ in the amount of 8.4 % was observed.

From the results of the quantitative analysis, alloy A contains a higher average length and amount of needle-like Fe phases compared to alloy B (Fig. 5b). The length of the needles has been shortened from 47 µm to 37 µm (27 % reduction).

The $Al_{15}(FeMn)_3Si_2$ phase size was measured at 354 µm^2. The shape of the Al_5FeSi phase in alloy B is significantly affected by the Mn addition when the expected transformation from the needle-like Al_5FeSi to skeleton-like or script-like $Al_{15}(FeMn)_3Si_2$ phase was achieved (Fig. 5b).

However, alloy B reaches higher average porosity and pore sizes compared to alloy A possibly due to Mn addition (Fig. 5c). Porosity increased from 2.6 to 6.3 % and the proportional size of casting defects increased.

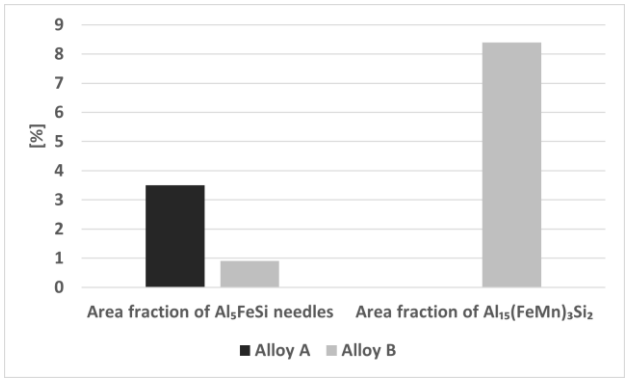

a) Effect of Mn on the amount of Fe-phases

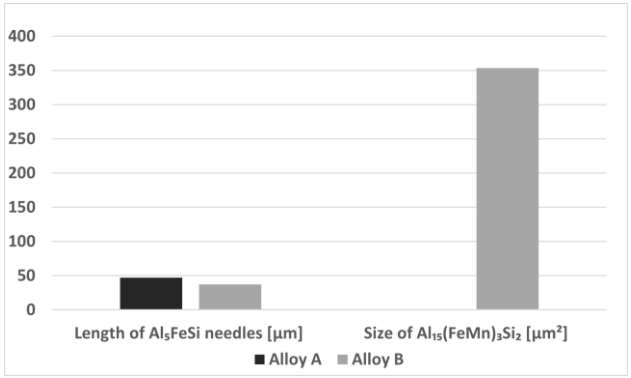

b) Effect of Mn on the length and size of Fe-phases

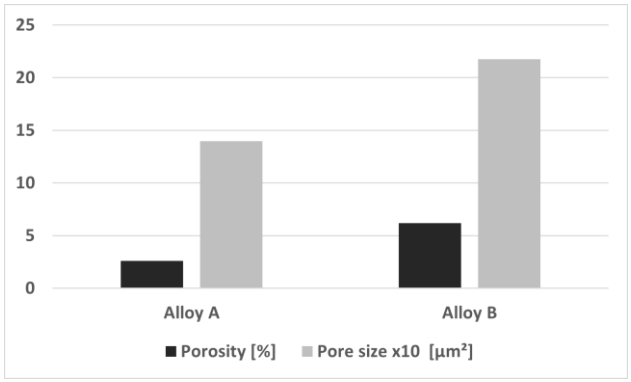

c) Effect of Mn on the porosity

Fig. 5. Quantitative analysis results of selected AlSi7Mg0.6 alloys parameters

In Fig. 6 the pores were observed in close contact with the Fe-needles (Fig. 6a) or in the 3D-platelets (Fig. 6b). This pore formation confirmed the studies of Brueckner-Foit [16] and Puncreobutr [23] of Fe-needles being surrounded by pores and acting as porosity nucleation sites.

The results of the quantitative analysis correspond with the work of the authors [14, 20]. As the Mn concentration increases, the size of the $Al_{15}(FeMn)_3Si_2$ particles increases too. This has probably a potentially detrimental effect on the porosity. The formation of large $Al_{15}(FeMn)_3Si_2$

phases will block interdendritic feed paths at high solid fractions.

At the same time, the authors [20] observed that at higher iron contents (Fe > 0.7 %), the Al_5FeSi-phase (even if it is low in quantity) participates in the nucleation of eutectic silicon, leading to a rapid deterioration of interdendritic permeability and consequently to formation of shrinkage porosity.

The higher porosity of alloy B may also be a result of the sludge phase's presence, thought that the primary sludge formed may act as nucleation sites for hydrogen porosity and/or prevent pore leakage [21].

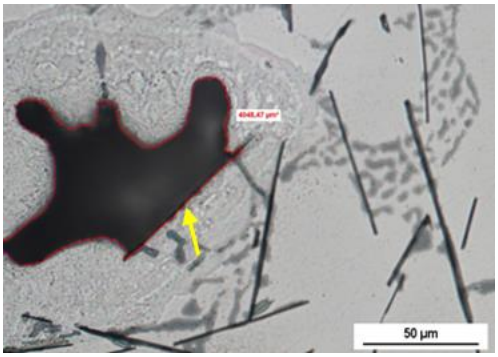

a) alloy A, etch. 95% H_2SO_4

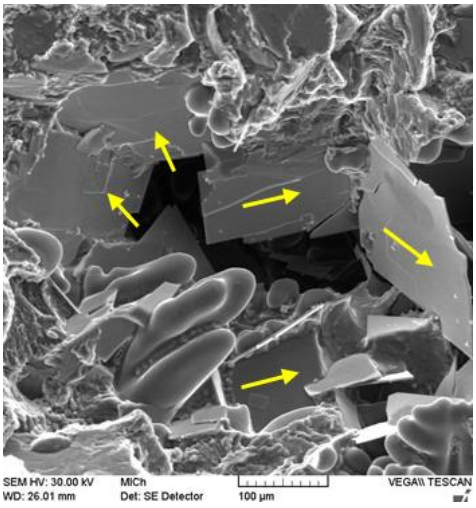

b) alloy A, SEM

Fig. 6. Pore formation surrounding Al_5FeSi phases (arrowed) in AlSi7Mg0.6 cast alloy

4. CONCLUSIONS

Both experimental materials with high iron content (1.2 %) have comparable main structural components. The microstructure consists of α-phase, eutectic and Fe- Mg-rich intermetallic phases. The amount and chemical composition of intermetallic phases depend on the type of experimental material. Differences between experimental materials, affected by addition of manganese, are as follows:

- Holding the recommended amount, Mn has a positive effect on elimination of negative needle-like β-Fe (Al_5FeSi phases).
- The addition of Mn causes the reduction of the number of the β-Al_5FeSi phases; leads to the transformation of brittle β-Fe platelets into less harmful α-Fe phases $Al_{15}(FeMn)_3Si_2$ with skeleton-like or Chinese script morphology, therefore, the lower risk of crack initiations is expected for alloy B. The occurrence of sludge phases has also been observed.
- However, Mn negatively affects the porosity - in alloy B with the addition of 0.66 wt.% Mn both the porosity and the average pore size significantly increased.

ACKNOWLEDGEMENT

The research was supported by Scientific Grant Agency of Ministry of Education of Slovak Republic and Slovak Academy of Sciences, VEGA 01/0398/19, KEGA 016ŽU-4/2020, project to support young researches at UNIZA, ID project 12715 (Kucharíková) and project 313011ASY4 "Strategic implementation of additive technologies to strengthen the intervention capacities of emergencies caused by the COVID-19 pandemic".

REFERENCES

[1] Vision 2050: European Aluminium's Contribution to the EU's Mid-Century Low-Carbon Roadmap. Available on-line on http://www.european-aluminium.eu/

[2] International Aluminium Institute. Available on-line on: https://www.lightmetalage.com/tag/international-aluminium-institute/

[3] D. Závodská, E. Tillová, I. Švecová, M. Chalupová, L. Kucharíková, J. Belan, The Effect of Iron Content on Microstructure and Porosity of Secondary AlSi7Mg0.3 Cast Alloy. *Periodica Polytechnica Transportation Engineering,* 47 (4), 2019: 283-289. https://doi.org/10.3311/PPtr.12101

[4] Circular Aluminium Action plan: A Strategy for Achieving Aluminiums Full Potential for Circular Economy by 2030. Available on-line on http://www.european-aluminium.eu/

[5] B. Zhou, S. Zhang, R. Lin, Y. Jiang, X. Lan, Microstructure evolution of recycled 7075

aluminum alloy and its mechanical and corrosion properties. *Journal of Alloys and Compounds,* 879, 2021: 160407. https://doi.org/10.1016/j.jallcom.2021.160407

[6] D. Brough, H. Jouhara, The aluminium industry: A review on state-of-the-art technologies, environmental impacts and possibilities for waste heat recovery. *International Journal of Thermofluids,* 1-2, 2020: 100007. https://doi.org/10.1016/j.ijft.2019.100007

[7] L. Kuchariková, E. Tillová, O. Bokůvka, Recycling and properties of recycled aluminium alloys used in the transportation industry. *Transport Problems*, 11, 2016: 117-122. https://doi.org/10.20858/tp.2016.11.2.11

[8] J. Svobodova, M. Lunak, M. Lattner, Analysis of the Increased Iron Content on the Corrosion Resistance of the AlSi7Mg0.3 Alloy Casting. *Manufacturing Technology*, 19(6), 2019: 1041-1046. https://doi.org/10.21062/ujep/415.2019/a/1213-2489/MT/19/6/1041

[9] C. M. Dinnis, J. A. Taylor, A. K. Dahle, Interactions between iron, manganese, and the Al-Si eutectic in hypoeutectic Al-Si alloys. *Metall Mater Trans*, A 37, 2006: 3283-3291. https://doi.org/10.1007/BF02586163

[10] D. Song, Y. Jia, Q. Li, Y. Zhao, W. Zhang, Effect of Initial Fe Content on Microstructure and Mechanical Properties of Recycled Al-7.0Si-Fe-Mn Alloys with Constant Mn/Fe Ratio. *Materials,* 15, 2022: 1618. https://doi.org/10.3390/ma15041618

[11] A. Miteva, A. Petrova, G. Stefanov, Surface Oxidation of Al-Si Alloys at Elevated Temperatures. *Applied Engineering Letters,* 6 (3), 2021: 105-110. https://doi.org/10.18485/aeletters.2021.6.3.3

[12] L. Kuchariková, E. Tillová, M. Samardziova, M. Uhríčik, J. Belan, I. Švecová, Quality Assessment of Al Castings Produced in Sand Molds Using Image and CT Analyses. *Journal of Materials Engineering and Performance*, 28, 2019: 3966-3973. https://doi.org/10.1007/s11665-019-04040-z

[13] J. A. Taylor, Iron-Containing Intermetallic Phases in Al-Si Based Casting Alloys. *Procedia Materials Science.* 1, 2012: 19-33. https://doi.org/10.1016/j.mspro.2012.06.004

[14] X. Cao, J. Campbell, Morphology of β-Al_5FeSi Phase in Al-Si Cast Alloys. *Materials Transactions,* 47 (5), 2006: 1303-1312. https://doi.org/10.2320/matertrans.47.1303

[15] A. Brueckner-Foit, M. Luetje, I. Bacaicoa, A. Geisert, M. Fehlbier, On the role of internal defects in the fatigue damage process of a cast Al-Si-Cu alloy. *Procedia Structural Integrity*, 7, 2017: 36-43. https://doi.org/10.1016/j.prostr.2017.11.058

[16] E. R. Wang, X. D. Hui, S. S. Wang, Y. F. Zhao, G. L. Chen, Improved mechanical properties in cast Al-Si alloys by combined alloying of Fe and Cu. *Materials Science and Engineering: A,* 527 (29-30), 2010: 7878-7884. https://doi.org/10.1016/j.msea.2010.08.058

[17] D. Bolibruchová, R. Podprocká, R. Pastirčák, K. Major-Gabryś, The role of Mn in aluminium alloys with a higher iron content. *Archives of Metallurgy and Materials,* 63 (4), 2018: 1883-1888. https://doi.org/10.24425/amm.2018.125119

[18] B. Madhav, A. A. Mohiuddin, M. Atifuddin, Comparison of Mechanical Properties of AlSiMg Alloy with Varied Composition. *International Journal of Engineering & Technology Research*, 4 (4), 2016: 12-19.

[19] K. Bangyikhan, Effects of Oxide film, Fe-rich phase, Porosity and their Interactions on Tensile Properties of Cast Al-Si-Mg Alloys. (Ph.D. thesis). *University of Birmingham*, 2005.

[20] S. Seifeddine, I. L. Svensson, The influence of Fe and Mn content and cooling rate on the microstructure and mechanical properties of A380-die casting alloys. *Metallurgical Science and Technology,* 27 (1), 2009: 11-20.

[21] A. Bjurenstedt, S. Seifeddine, A. Jarfors, The effects of Fe-particles on the tensile properties of Al-Si-Cu alloys. *Metals*, 6 (12), 2016: 314. https://doi.org/10.3390/met6120314

[22] C. Puncreobutr, P. D. Lee, K. M. Kareh, T. Connolley, J. L. Fife, A. B. Phillion, Influence of Fe-rich in-termetallics on solidification defects in Al–Si–Cu alloys. *Acta Materialia*, 68, 2014: 42-51. https://doi.org/10.1016/j.actamat.2014.01.007

[23] L. Stanček, B. Vanko, A. I. Batyšev, Structure and properties of silumin castings solidified under pressure after heat treatment. *Metal Science and Heat Treatment*, 56, 2014: 197-202.

https://doi.org/10.1007/s11041-014-9730-0

[24] R. Dunn, Aluminum melting problems and their influence on furnace Selection. *Die Cast. Eng*. 1965: 8-16.

[25] L. Ceschini, A. Morri, S. Toschi, A. Bjurenstedt, S. Seifeddine, Influence of Sludge Particles on the Fatigue Behavior of Al-Si-Cu Secondary Aluminium Casting Alloys. *Metals*, 8 (4), 2018: 268. https://doi.org/10.3390/met8040268